


# Rotary LED Transmitter for Improving Data Transmission Rate of Image Sensor Communication

Shintaro Arai , *Member, IEEE*, Zhengqiang Tang , *Student Member, IEEE*, Akinori Nakayama, Haruhiro Takata, and Tomohiro Yendo, *Member, IEEE*

**Abstract**—This study focuses on image sensor communication (ISC), which is a form of visible light communication, using a light-emitting diode (LED) and a camera as the transmitting and receiving device, respectively. In an ISC system, the receiver captures optical signals transmitted by blinking LEDs as an image and demodulates the data using the captured image. The ISC system can spatially separate signals and noises in the image, thus providing superior anti-interference ability. However, because the speed of ISC depends on the shooting speed of the camera, the receiver suffers from a low data transmission rate when a low-speed camera is used. To improve the data rate of ISC, we have developed a rotary LED transmitter. This transmitter cylindrically rotates the blinking LEDs during the exposure time of the camera. The camera captures multiple blinking states of LEDs as afterimages in a single image, thereby increasing the amount of data received per image. In this paper, we propose an ISC system using a rotary LED transmitter and present an experiment for the evaluation of the data rate. The result indicates that the data rate of the rotary LED transmitter is 60 times that of the conventional method.

**Index Terms**—Visible light communication, image sensor communication, optical camera communication, rotary LED transmitter, afterimage of LED light.

## I. INTRODUCTION

THE invention of white light-emitting diodes (LEDs) in the 1990 s revolutionized the traditional lighting industry [1]. LEDs are characterized by their high brightness, low power consumption, and long life span [2]. Owing to these advantages, the use of LEDs has increased rapidly since their mass production began at the end of the 20th century. With the extensive use of LEDs, a new wireless communication technique called visible light communication (VLC) [3] has been developed.

VLC is a type of optical wireless communication technology [4] that transmits information using electromagnetic waves in the visible spectrum. In VLC, visible light with a wavelength of 380–780 nm is used. In contrast, the wavelength of radio

waves used in practical radio communication ranges from approximately 0.1 mm to several kilometers, which is several hundred to several tens of billions of times the wavelength of VLC. Owing to this difference in wavelength, VLC has the following features:

- The shorter the wavelength, the less the radio waves' diffraction. Therefore, visible light travels almost straight ahead, and the transmitter and receiver can easily recognize each other. Communication with a specific entity is possible, thus enabling a highly directional communication [5].
- Because the communication range is visible, it is easy to prevent information from being delivered to unintended recipients, thus providing a high level of communication security [6].
- Owing to the visibility of communication range, the visible light signal of VLC can also be used for positioning services [7]–[9].
- The bandwidth of VLC does not require a license because there are no legal restrictions.
- As long as the light is not too intense, it is safe and has no effect on the human body or precision instruments [10].
- Practical radio communication and VLC can be used simultaneously without interference. In the event of a disaster, information can be delivered safely and quickly to those in need through multiple communication channels [11].
- Communication using VLC can be achieved in special environments, such as underwater, where radio waves attenuate rapidly [12]–[14].

In VLC, optical signals are transmitted by blinking LEDs. The blinking frequency of an LED can be up to 1 MHz [6] while the refresh rate of a computer screen is approximately 100 Hz. This implies that we can modulate the blinking frequency of an LED at a high speed that is undetectable to the human eye.

To detect optical signals transmitted by LEDs, two types of light-receiving devices are typically used in VLC: a photodiode (PD) and an image sensor. A PD is a semiconductor device that converts light into electric current. Owing to the fast response time, VLC systems using a PD can easily realize high-speed communication. However, because a PD is sensitive to light, it does not distinguish well between signal and nonsignal light sources when used outdoors or in other environments with strong background light, thus resulting in poor communication quality. An image sensor (camera) converts light to electrical signals to be output as an image. Image sensor communication

Manuscript received April 29, 2021; revised June 9, 2021; accepted July 11, 2021. Date of publication July 19, 2021; date of current version August 17, 2021. This work was supported in part by JSPS KAKENHI under Grants JP17K18282 and JP21K11948, and in part by the joint research program of the Institute of Materials and Systems for Sustainability, Nagoya University. (*Corresponding author: Shintaro Arai.*)

Shintaro Arai and Akinori Nakayama are with the Okayama University of Science, Okayama 700-0005, Japan (e-mail: arai@ee.ous.ac.jp).

Zhengqiang Tang is with the Nagoya University, Nagoya 464-8603, Japan.

Haruhiro Takata and Tomohiro Yendo are with the Nagaoka University of Technology, Nagaoka 940-2188, Japan.

Digital Object Identifier 10.1109/JPHOT.2021.3097772

(ISC) is a scenario where a VLC system that uses an image sensor as a receiver is used [15]–[19]. ISC is often referred to as an optical camera communication (OCC). Both ISC and OCC refer to VLC technology that uses a camera (image sensor) as a receiver, and the only clear difference between the two communication systems is their terminology [20]. In ISC, the LED luminance is detected and extracted as a pixel from the captured image [21]. Then, the data are demodulated using the extracted pixel. Because the data are demodulated from a two-dimensional captured image, ISC can spatially separate signals and noises in the image, thereby providing superior anti-interference ability [22]–[24].

In this paper, we focus on ISC. As mentioned earlier, ISC systems are extremely robust to background noise owing to their spatial separation capability. However, achieving a high data transmission rate remains a great challenge in ISC. Because data are demodulated from the captured image, the shooting speed of the camera affects the speed of ISC. The amount of data received in a unit of time depends largely on how many images the camera captures per second. However, the shooting speed of a commercial camera usually ranges from 30 frames per second (fps) to 60 fps. We assume that a transmitter LED modulated by ON–OFF keying (OOK) is recognized by a receiver camera with a shooting speed of 60 fps. Moreover, the transmitter and receiver are fully synchronized. The data transmission rate in this case is 60 bits per second (bps), which is extremely low for information transmission.

Although this problem can be solved by using a dedicated high-speed camera, the high cost makes it impractical for general-purpose applications. Therefore, the challenge is to improve the data transmission rate of ISC using commercially available cameras [11]. Various schemes, such as rolling shutter-type ISC [25] and polygon-mirror-based ISC [26], have been proposed to increase the data transmission rate. We introduce these two schemes in Section II and discuss their advantages and disadvantages.

The purpose of this study is to improve the speed of ISC, where a low-cost camera is used as the receiver. In particular, we propose a new transmitter referred to as “a rotary LED transmitter”<sup>1</sup> for ISC systems, as illustrated in Fig. 1. The rotary LED transmitter increases the data transmission rate of ISC by utilizing the afterimage of LED light due to the relative motion of the LED and the camera.

The remainder of this paper is organized as follows. In Section II, we introduce the related studies that aim to increase the speed of ISC. In Section III, we describe the structure of the proposed rotary LED transmitter, and explain the principle of communication speed improvement by the proposed transmitter. In Section IV, we present an ISC system model based on the rotary LED transmitter and the projection model of the transmitter. We evaluate the proposed system by a computer simulation and an experiment in Sections V and VI, respectively, and discuss the results. Finally, we summarize the contributions of this study in Section VII.

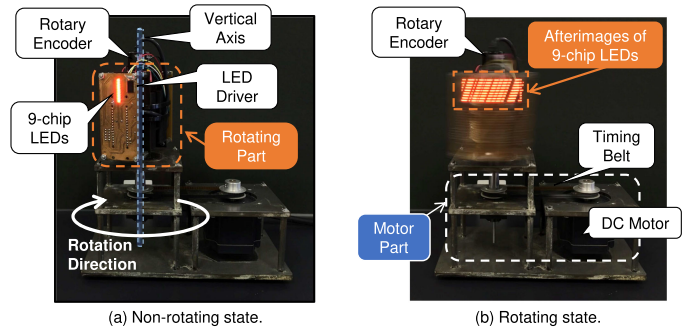


Fig. 1. Non-rotating and rotating states of the rotary LED transmitter. This transmitter increases the data transmission rate of ISC by utilizing the afterimages of LED lights due to the relative motion of the LED and camera.

## II. RELATED WORK

### A. Rolling Shutter-Type ISC Scheme

Most smartphone cameras use rolling shutter-type image sensors. As discussed in the introduction, these commercial smartphone cameras usually capture 30–60 fps. According to the IEC 62943:2017 standard [28], which was produced by the International Electrotechnical Commission (IEC) in 2017, the transmitter LED is modulated at 9.6 kHz. However, smartphone cameras operating at 30–60 fps cannot receive transmission signals from LEDs modulated at 9.6 kHz. In 2012, Danakis *et al.* proposed a rolling shutter-type ISC scheme that utilized the line-scan mechanism of the rolling shutter-type image sensor [25].

Here, we describe the line-scan mechanism and introduce the fundamental principle of ISC based on the rolling shutter method. We consider one row of pixels in an image sensor to be one scan line, and there are multiple scan lines per sensor. The rolling shutter exposes the scan lines at the top of the sensor from top to bottom and reads the electric charge according to the amount of light. Each scan line is scanned sequentially with a different timing,  $T_l$ .

As illustrated in Fig. 2, when the camera captures an LED modulated at the rate of  $1/T_l$ , each line is projected as a striped pattern in the row direction. In this case, each strip indicates a blinking state of the LED, and data can be demodulated from the strips. For example, we assume that a rolling shutter-type image sensor with 1080 scan lines captures an LED at a shooting speed of 30 fps. The maximum sampling rate is  $1/T_l = 30 \times 1080 = 32.4$  kHz, which indicates that rolling shutter-type ISC can receive the transmitter LED modulated at 9.7 kHz. However, this scheme requires the light from LED to be received over a large area of the sensor to achieve a high data transmission rate.

### B. Polygon Mirror-Based ISC Scheme

In this subsection, we introduce an ISC scheme that uses a polygon mirror to improve the data transmission rate. A polygon mirror, also called “a rotating polyhedron,” has a number of mirror surfaces parallel or inclined to the axis of rotation, and is used for scanning a light beam. The ISC scheme based on a

<sup>1</sup>We briefly introduced this transmitter in [27].

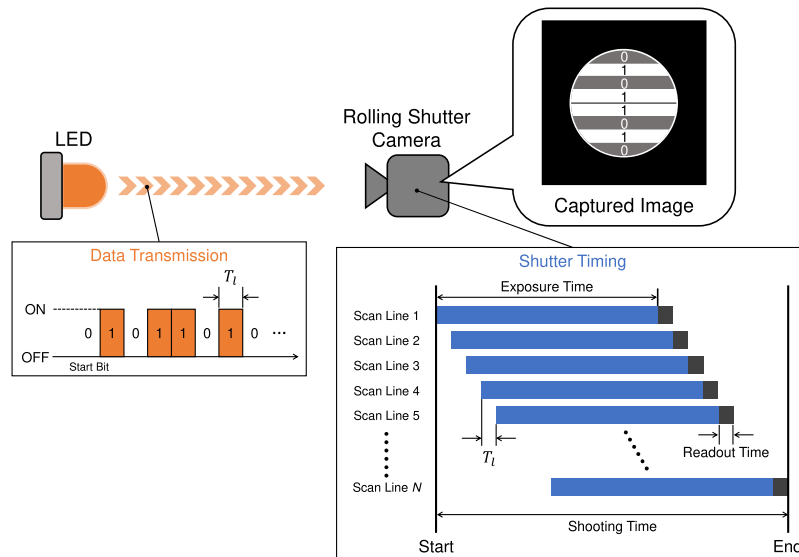


Fig. 2. Rolling shutter-type ISC scheme. The rolling shutter sequentially exposes the scan lines of the image sensor from top to bottom with different timings,  $T_i$ . Each scan line is projected as a striped pattern, which indicates the blinking state of the LED, in the row direction when the camera captures an LED modulated at the rate of  $1/T_i$ . The data are then demodulated from the strips.

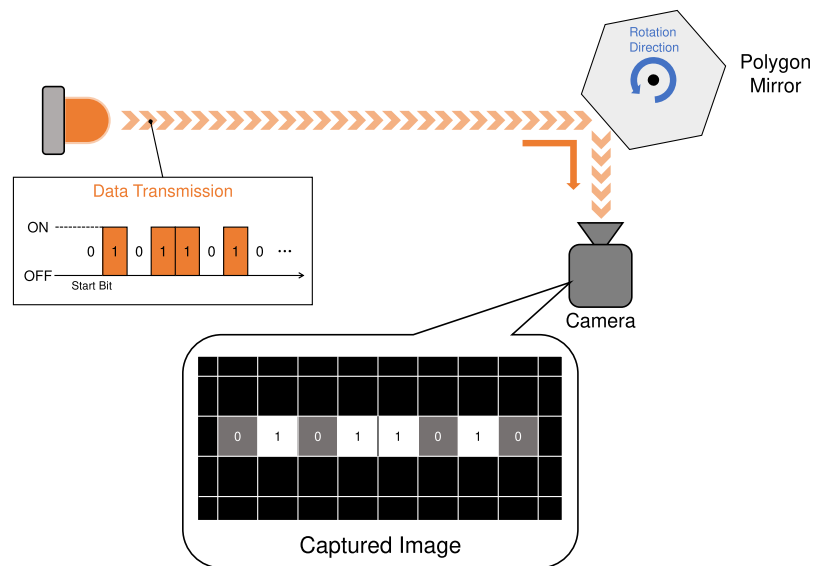


Fig. 3. Polygon mirror-based ISC scheme. The polygon mirror is placed in the front of the image sensor and rotates at a constant speed. It scans the incoming light and reflects it onto the image sensor. In this case, the direction of the LED blinking is converted from the time axis to the spatial axis of the image. The data are then demodulated from the reflected lights.

polygon mirror was proposed by Imai *et al.* in 2016 [26]. This scheme was designed to increase the data transmission rate for intervehicle ISC, in which vehicle tail lamps and image sensors were used as transmitters and receivers, respectively.

The receiving devices used in polygon-mirror-based ISC consist of a low-speed commercial image sensor, a polygon mirror, and a decoder. As illustrated in Fig. 3, the polygon mirror is placed in the front of the image sensor and rotates at a constant speed. The polygon mirror scans incoming light and reflects it onto the image sensor. By scanning the LED light source that blinks at high speed on an image sensor using a rotating polygon mirror, the direction of the blinking of LEDs

is converted from the time axis to the spatial axis of the image. As a result, the number of bits recorded per image increases, and the communication speed of each LED light source effectively increases.

In an experiment using image sensors with the same shooting speed [26], the communication method using a polygon mirror achieved a data transmission rate ten times higher than that achieved by a conventional method. Imai *et al.* [26] also reported a bit error rate (BER) that is practical for low-noise environments. However, because the incoming light is reflected owing to the use of a rotating polygon mirror in the front of the camera, it is difficult to capture an image without distortion.

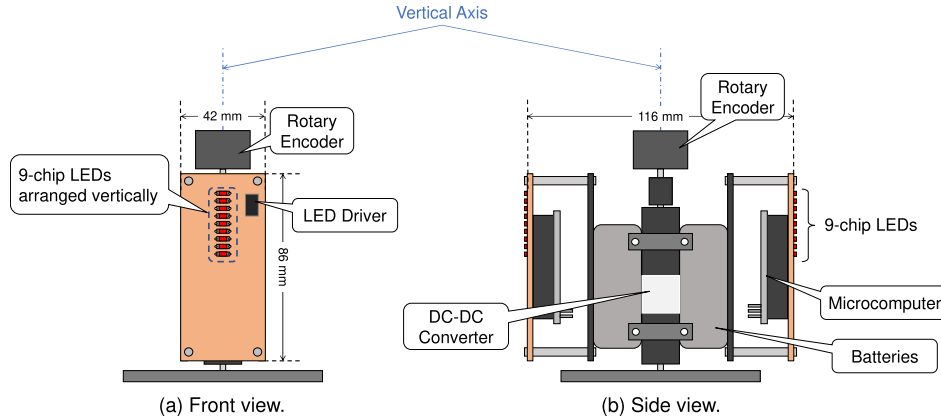


Fig. 4. Front and side views of the rotary LED transmitter. The rotating part consists of 9-chip LEDs, an LED driver, a microcomputer, and a rotary encoder. The 9-chip LEDs are arranged in a vertical row, and they rotate with the rotary encoder around a vertical axis. While the transmitter rotates, the rotary encoder outputs a clock signal for each rotation angle. The microcomputer controls the blinking patterns of the 9-chip LEDs via LED drivers according to the clock signals from the rotary encoder.

TABLE I  
MAIN COMPONENTS OF THE ROTARY LED TRANSMITTER

Components	Specification
LED	SML-M13UTT86
LED driver	TLC5922
Microcomputer	Arduino Nano
Rotary encoder	E6A2-C
DC-DC converter	CC3-0505 SF-E
DC motor	BLEM-23-A
Motor driver	BLED3A

### III. ROTARY LED TRANSMITTER

#### A. Structure of the Rotary LED Transmitter

To improve the speed of ISC using commercially available cameras, we develop a new transmitter called “a rotary LED transmitter.” The rotary LED transmitter consists of two parts: a rotating part and motor part. The motor part provides the rotation power for the rotating part through a direct current (DC) motor and a timing belt. The main components of the transmitter are listed in Table I.

The rotating part consists of 9-chip LEDs, an LED driver, a microcomputer, and a rotary encoder. To ensure the stability of the rotational motion, we adopted a symmetrical structure for the rotating part. Figs. 4(a) and (b) present the front and side views of this part, respectively. The 9-chip LEDs are arranged in a vertical row and rotate with the rotary encoder around a vertical axis. A rotary encoder, a microcomputer, and an LED driver are used to control the blinking of the LEDs. A rotary encoder is a device that outputs signals according to the angular position of a shaft, and in this study, it is used to generate a clock to control the blinking pattern of an LED for each rotation angle. While the transmitter rotates, the rotary encoder outputs a clock signal for each rotation angle. The microcomputer controls the blinking patterns of the 9-chip LEDs via LED drivers according to the clock signals from the rotary encoder.

#### B. Data Rate Improvement by Using the Rotary LED Transmitter

The main principle of our proposed method to improve the data transmission rate of ISC is to increase the number of received bits of data per captured image by using the afterimages of LED lights. It is well known that the movement of an object during the exposure time of a camera produces an afterimage in the captured image [29]. The generation of afterimages should be generally avoided because they degrade the quality of the captured image, thereby reducing the data demodulation performance of ISC systems. However, in the field of image processing, there is a method to track the movement of an object from the beginning to the end of the camera exposure time by intentionally using afterimages [30].

Based on this concept, we propose that changes in the blinking of LEDs during the camera exposure time can also be stored as afterimages. To generate afterimages of LED lights, we rotate the blinking LEDs. We assume that the exposure time of the camera is sufficiently lower than the rotation speed of the transmitter and the blinking speed of the LEDs. In this way, the number of received data bits per captured image is increased because the LEDs blink according to the data at a speed that is faster than the shooting speed of the camera. In this study, we assume that the camera’s exposure time is the same as its shooting time. This implies that the time difference between the successive frames caused by the opening and closing of the camera aperture can be ignored.

Now, we demonstrate the number of bits of data received per captured image when one LED is fixed (conventional method) and when it is rotating (proposed method) during the exposure time of the camera. First, we examine the case in which the position of the LED is fixed, as illustrated in Fig. 5. In this case, the camera receives the blinking state of the LED for each captured image. Let  $F_L$  [Hz] and  $F_c$  [Hz] denote the blinking frequency of the transmitter LED and the shooting frequency of the receiver camera, respectively. Note that both the shooting speed and  $F_c$  indicate the number of frames that the camera captures per second. We assume that the LED and camera are fully synchronized. This signifies that the changes in the timing



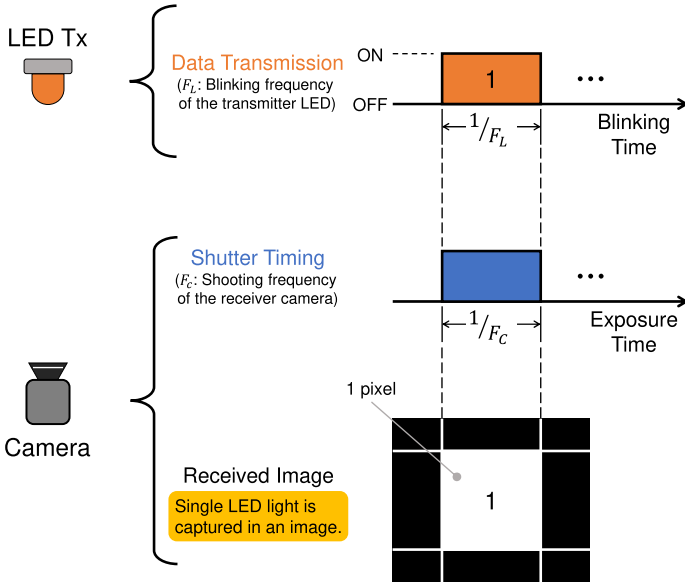


Fig. 5. Capturing an LED when its position is fixed. To obtain the changes in LED blinking, the camera must capture one LED blinking state per frame. In this case, the camera shooting frequency ( $F_c$ ) must be equal to the LED blinking frequency ( $F_L$ ).

of the LED blinking match the timing of the camera shutter opening. To obtain the changes in LED blinking, the camera must capture one LED blinking state per frame. Therefore, when fixing the position of the LED,  $F_L$  and  $F_c$  must satisfy the following relationship to achieve communication in ISC:

$$F_c = F_L. \quad (1)$$

For example, if an LED blinks three times, the camera requires three frames to capture each blinking state.

Now, we focus on the case in which the LED is rotating, as illustrated in Fig. 6. Here, let  $\Delta\theta$  [°] denote the rotation angle for changing the blinking state of an LED. The time taken for a 360° rotation of an LED is equal to the exposure time of the camera. In this case,  $F_L$  and  $F_c$  have the following relationship:

$$F_c = \frac{\Delta\theta}{360} F_L. \quad (2)$$

By comparing Eq. (2) with Eq. (1), we observe that the camera shooting frequency is not required to be equal to the LED blinking frequency if an LED is rotating. By setting  $\Delta\theta$  to a value smaller than 360°, the camera can capture an LED that blinks faster than its shooting speed. In the captured image, the change in the blinking state is saved as the afterimages, as illustrated in Fig. 6. When the LED rotates and simultaneously blinks in the front of the receiver camera, the number of blinking states that the camera can capture in one frame is up to  $180^\circ/\Delta\theta$ . Note that an LED blinking state indicates received data.

Figs. 7(a) and (b) display the captured images when 9-chip LEDs are fixed and when they are rotating, respectively. Here,  $\Delta\theta$  was set to 1°. As illustrated in Fig. 7, if the LEDs are fixed, the camera captures only 9 blinking states per image. If blinking LEDs are rotated during the exposure time of the camera, the afterimages of the LED lights rotated by 180° can

be captured in a single image because the LED blinking state changes every 1°. This means that 1620 ( $= 180^\circ \times 9$ ) blinking states are captured at once. Note that in both cases, the number of LEDs used for data transmission is the same. When the positions of the LEDs are fixed, the camera requires several images to capture each blinking state. By using the afterimage of the LED light, these blinking states can be captured in a single image. The amount of received data is increased for every captured image, thereby improving the speed of ISC.

With the rotary LED transmitter, the shooting frequency  $F_c$  of the receiver camera is no longer required to match the blinking frequency  $F_L$  of the transmitter LED. Therefore, it is possible to achieve high-speed ISC despite the use of inexpensive, commercially available cameras with low shooting speeds. In addition, the number of received LEDs (i.e., bits of received data) can be changed by changing the value of  $\Delta\theta$ . In conventional ISC systems, an LED array transmitter is typically used, which is a matrix of LEDs. The number of LEDs in the array transmitter is constant, and the position of each LED is fixed. When the LED array transmitter is used to transmit signals, the number of bits of data that the camera receives per image is fixed. Compared with the conventional transmitter, the rotary LED transmitter can freely change the number of LED blinking states per transmission, thereby changing the number of received data bits per image. Therefore, the rotary LED transmitter has a high degree of freedom in terms of the data transmission rate.

In the proposed transmitter, even if a DC motor not having stable rotation speed is used in the transmitter and jitter occurs, it hardly affects the data transmission. The rotary LED transmitter uses the rotary encoder to change the blinking state of the LEDs at every  $\Delta\theta$  [°]. Therefore, the blinking state is controlled only by the angle change caused by the rotation and not by the rotation speed. Using the rotary encoder guarantees the robustness of the data transmission when jitter occurs if the motor speed is unstable.

#### IV. ISC SYSTEM USING THE ROTARY LED TRANSMITTER

##### A. System Model

Fig. 8 illustrates the proposed system model of ISC using the rotary LED transmitter. As mentioned in Section III-A, the rotary LED transmitter has 9-chip LEDs arranged in a vertical row. To transmit information 360° in all directions, the transmitter rotates cylindrically around a vertical axis, as illustrated in Fig. 9. The blinking of each LED changes every  $\Delta\theta$  degrees of rotation.

In this study, we use OOK as the modulation method. Binary data are modulated by a microcomputer and allocated to each LED via an LED driver. The rotary LED transmitter changes the LED blinking pattern (i.e., transmission signal) every  $\Delta\theta$  degrees of the rotation angle, and transmits the same signal every  $\alpha$  [°]. The transmission pattern continues for one rotation of the transmitter; after which, the transmitter adopts a different transmitting signal pattern. To identify the angular range of data transmission, 9-chip LEDs are all in the ON state every  $\alpha$ . In this study, the blinking pattern in which all LEDs are in the ON state is called “Guard.”

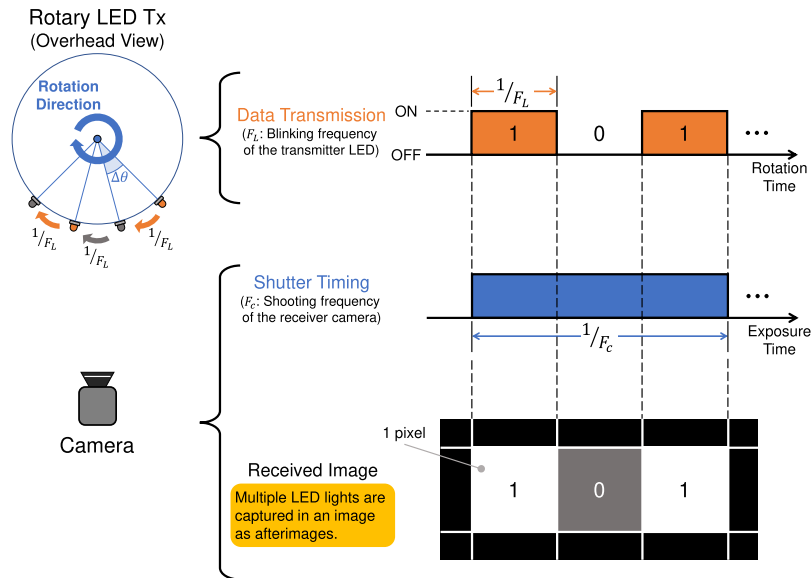


Fig. 6. When an LED is rotating during the exposure time, the camera captures the change in the blinking state as afterimages in one frame. In this case, the camera shooting frequency ( $F_c$ ) is not required to be equal to the LED blinking frequency ( $F_L$ ).

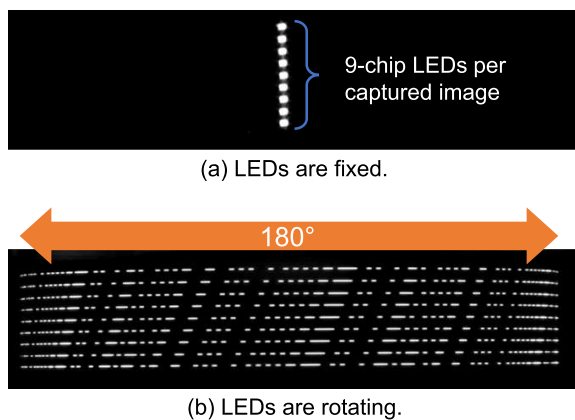


Fig. 7. Captured images when 9-chip LEDs are in a fixed position and rotating. Here,  $\Delta\theta$  was set to  $1^\circ$ . When the LED positions are fixed, the camera captures 9 blinking states per frame. When the LEDs rotate and change the blinking state every  $1^\circ$ , the camera captures 1620 ( $=9 \times 180^\circ$ ) blinking states in a single image.

The receiving device is composed of a camera, an image processing unit, and a decoder. The camera receives LED light transmitted through the spatial channel and outputs it as a captured image. Then, the image processing unit detects the position of the LEDs and extracts the luminance value of each LED from the captured image as a pixel. Finally, the decoder demodulates the data with the extracted pixel.

Notably, the proposed receiver can receive the transmitted data without synchronizing the timings of the transmitter rotation and receiver shooting. The receiver captures  $180^\circ$  of the afterimages of the LED lights generated by the transmitter rotation in one frame (Fig. 7(b)). From the captured image, we can then extract the afterimages of the LED lights for  $\alpha$ , which are sandwiched between the Guards, using image processing.

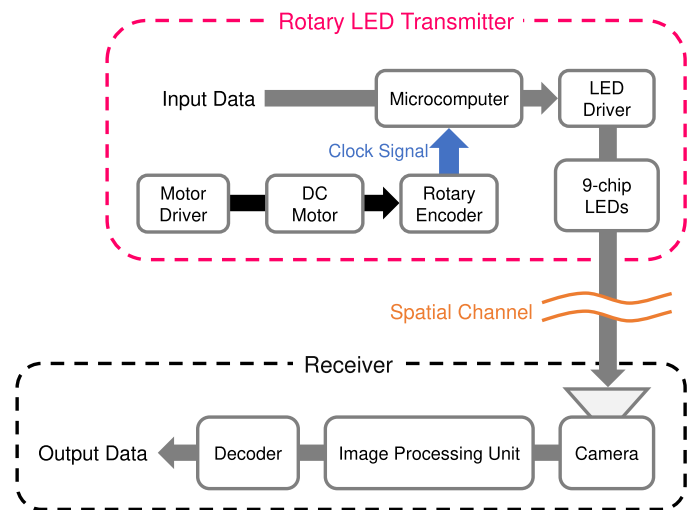


Fig. 8. Image sensor communication system model based on the rotary LED transmitter.

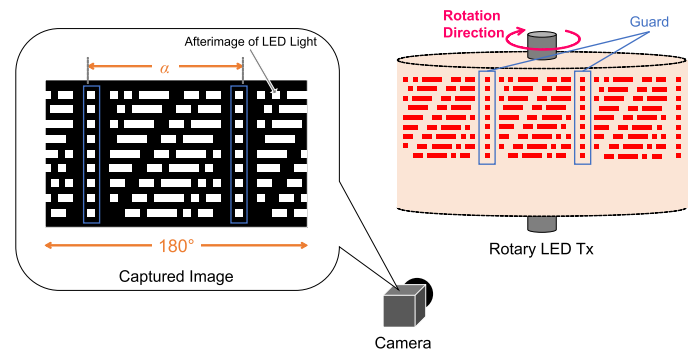


Fig. 9. Data transmission angular range of rotary LED transmitter. To identify the angular range of the data transmission, all the 9-chip LEDs are in the ON state for every  $\alpha$  [ $^\circ$ ]. In this study, the blinking pattern in which all LEDs are in the ON state is called “Guard.”

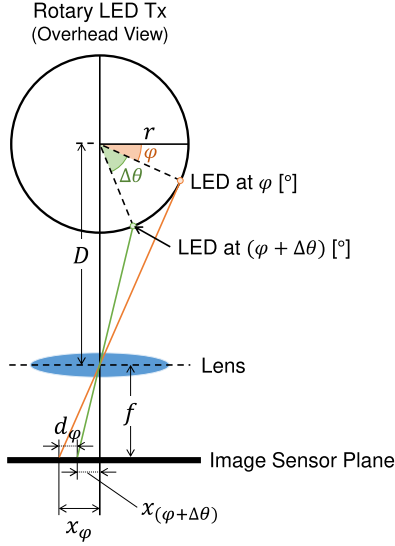


Fig. 10. The projection model of the rotary LED transmitter.

### B. Projection Model of the Rotary LED Transmitter

In this subsection, we present the projection model of the rotary LED transmitter and discuss the relationship between the data transmission angular range  $\alpha$  and predicted demodulation performance. As described in Section III-B, the camera can capture LED blinking states of  $180^\circ$  in a single frame. To achieve the maximum data transmission rate, the data transmission angular range  $\alpha$  should be as close to  $180^\circ$  as possible to allow the largest number of afterimages to be captured at once. However, the LED light overlaps on both sides of the captured image owing to the cylindrical rotation. The closer  $\alpha$  is to  $180^\circ$ , the more difficult it is to distinguish the blinking states of the LEDs, thereby reducing the demodulation performance. To ensure high demodulation performance and maximize the data transmission rate, an optimal  $\alpha$  is required. The data transmission rate is discussed in detail in Section VI.

Fig. 10 presents the projection model of the rotary LED transmitter, where the rotation radius of the transmitter is denoted by  $r$  [m]. We assume that the LED starts to change its blinking state at rotation angle  $\varphi$  [°]. The same blinking state continues until the angle  $\varphi + \Delta\theta$  is reached. In this projection model, we set  $\varphi + \Delta\theta \leq 180^\circ$ . Let  $x_\varphi$  [pixels] denote the length of the LED light in the image at rotation angle  $\varphi$ , as illustrated in Fig. 10. Letting  $k_x$  [m] denote the physical size of a pixel,  $x_\varphi$  is calculated as follows:

$$x_\varphi = \frac{f \cdot r \cos \varphi}{k_x (D - r \sin \varphi)}, \quad (3)$$

where  $f$  [m] and  $D$  [m] represent the focal length of the lens and the communication distance, respectively. Letting  $x_{(\varphi+\Delta\theta)}$  [pixels] denote the length of the LED light in the image at a rotation angle of  $\varphi + \Delta\theta$ ,  $x_{(\varphi+\Delta\theta)}$  is calculated as follows:

$$x_{(\varphi+\Delta\theta)} = \frac{f \cdot r \cos(\varphi + \Delta\theta)}{k_x (D - r \sin(\varphi + \Delta\theta))}. \quad (4)$$

Let  $d_\varphi$  [pixels] denote the length of the LED light in the image corresponding to the  $\varphi$ -th degree of the LED rotation. This

TABLE II  
SIMULATION PARAMETERS

Number of LEDs ( $N_L$ )	9
Blinking angle ( $\Delta\theta$ )	$1^\circ$
Data angular range ( $\alpha$ )	$45^\circ, 60^\circ, 90^\circ, 120^\circ$
Modulation method	ON-OFF keying (OOK)
Optical channel matrix	2D Gaussian filter
Filter size	$3 \times 3$
Variance of the Gaussian filter ( $\sigma_g^2$ )	1.0
Background noise $E_b/N_0$	Additive White Gaussian Noise (AWGN) 5 dB
LED light-emitting area	$0.285 \mu\text{m} \times 0.285 \mu\text{m}$
LED rotating radius ( $r$ )	$58 \times 10^{-3}$ m
Vertical interval of LEDs	2.85 mm
Focal length of lens ( $f$ )	$35 \times 10^{-3}$ m
Pixel size ( $k_x$ )	$4.5 \times 10^{-6}$ m
Communication distance ( $D$ )	0.5–4.0 m
Trials	10,000

length  $d_\varphi$  can be obtained by computing the absolute value of the difference between  $x_\varphi$  and  $x_{(\varphi+\Delta\theta)}$  as follows:

$$d_\varphi = |x_\varphi - x_{(\varphi+\Delta\theta)}|. \quad (5)$$

Here, we consider the rotating radius  $r$ , the blinking angle  $\Delta\theta$ , and the focal length  $f$  as the intrinsic parameters of the proposed system. The value of  $d_\varphi$  varies depending on the parameters  $\varphi$  and  $D$ . We change the value of  $\varphi$  in the range of  $0^\circ$  to  $(180 - \Delta\theta)$  [°] and calculate  $d_\varphi$  every  $\Delta\theta$ . Then, we compare the calculated  $d_\varphi$  with the pixel size. Finally, we count the number of  $d_\varphi$  values and determine the data transmission angular range  $\alpha$  for each communication distance  $D$  as follows:

$$\begin{cases} d_\varphi \geq 1 & \text{distinguishable} \\ \text{otherwise} & \text{overlapped} \end{cases}. \quad (6)$$

Here,  $d_\varphi$  that is smaller than 1 indicates that the LED lights are overlapped in the captured image. However, the actual effective  $\alpha$  is smaller than the calculated  $\alpha$  owing to the size of the LED and light diffusion. In this study, we demonstrate the demodulation performance with different  $\alpha$  values in Section V through computer simulations and explore the optimal value of  $\alpha$ .

## V. SIMULATION

The data demodulation performance of the proposed ISC system was evaluated through a computer simulation and an experiment. In this section, we present the simulation evaluation.

### A. Simulation Conditions

Table II lists the simulation parameters. To change the LED blinking state, on the transmitter side, the blinking angle ( $\Delta\theta$ ) was set to  $1^\circ$ , and the data transmission angular range ( $\alpha$ ) was set to  $45^\circ, 60^\circ, 90^\circ$ , and  $120^\circ$ . This signifies that the data transmission range was limited to  $\pm(\alpha/2)$  degrees from the center of the captured image. The binary input data were randomly generated and were modulated by OOK. The ON

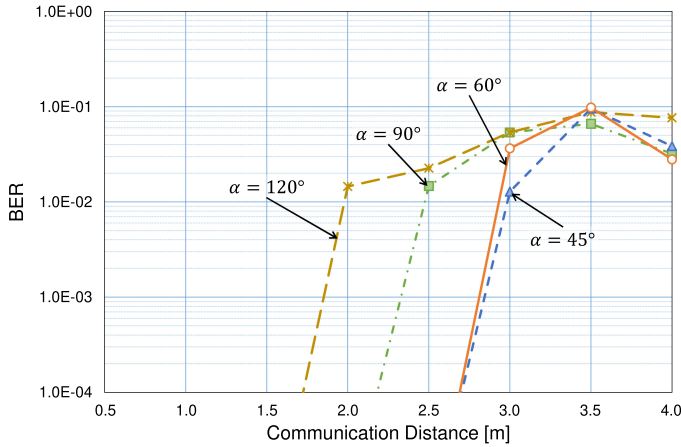


Fig. 11. BER plotted against the communication distance with constant  $\sigma_g^2$  ( $= 1.0$ ) and constant  $E_b/N_0$  ( $= 5$  dB). The data angular range ( $\alpha$ ) was set to  $45^\circ$ ,  $60^\circ$ ,  $90^\circ$ , and  $120^\circ$ .

and OFF states of the LED indicated the bits “1” and “0,” respectively. The modulated data were then transmitted by blinking LEDs.

The optical channel matrix, which is based on the two-dimensional Gaussian filter with a  $3 \times 3$  kernel, is defined as follows:

$$G_{i,j} = \frac{1}{2\pi\sigma_g^2} \exp\left(-\frac{i^2 + j^2}{2\sigma_g^2}\right), \quad (7)$$

where  $\sigma_g^2$  is the variance of the filter, and  $i$  and  $j$  are the vertical and horizontal components of the distance from the origin, respectively. With an increase in the value of  $\sigma_g^2$ , the degradation of the received image becomes significant. In this simulation, we set  $\sigma_g^2$  to 1.0. After filtering, additive white Gaussian noise (AWGN) was added to the degraded image as the ambient light noise. Let  $E_b/N_0$  denote the ratio of the transmit signal energy to the noise density per bit. With an increase in the value of  $E_b/N_0$ , the background noise interference increases. In this simulation, we set  $E_b/N_0$  to 5 dB.

The received image was pseudo-generated according to the communication distance by using the parameters of the rotary LED transmitter and camera presented in Table II. This implies that the size of the LED afterimage in the pseudo-received image was almost the same as that in the actual experiment. The communication distance was set in the range of 0.5–4.0 m. We measured the BER when data were transmitted 10000 times every 0.5 m.

### B. Simulation Result

Fig. 11 presents the BER plotted against the communication distance with constant  $\alpha$  ( $= 45^\circ$ ,  $60^\circ$ ,  $90^\circ$ , and  $120^\circ$ ). The values of  $\sigma_g^2$  and  $E_b/N_0$  were set to 1.0 and 5 dB, respectively. The vertical and horizontal axes represent the communication distance and the BER of various  $\alpha$  values, respectively.

First, we focus on the BER curve of  $\alpha = 120^\circ$ . The rotary LED transmitter sent more LED blinking states when  $\alpha = 120^\circ$  than when  $\alpha = 45^\circ$ ,  $60^\circ$ , and  $90^\circ$ . With an increased number of blinking states sent, more bits of data are transferred. However, in this case, the first demodulation error occurred at

TABLE III  
EXPERIMENTAL PARAMETERS

Number of LEDs ( $N_L$ )	9
Blinking angle ( $\Delta\theta$ )	$1^\circ$
Data angular range ( $\alpha$ )	$60^\circ$
Rotation speed of transmitter ( $S_r$ )	300 rpm
Rotation radius of transmitter ( $r$ )	$58 \times 10^{-3}$ m
Modulation method	ON–OFF keying (OOK)
Camera	UI-3250ML
Focal length of lens ( $f$ )	$35 \times 10^{-3}$ m
Aperture	F8
Shooting speed of the camera	5 fps
Lens filter	ND8
Communication distance ( $D$ )	0.5–4.0 m

approximately 1.75 m. This implies that when  $\alpha$  was set to  $120^\circ$  the error-free transmission distance was approximately 1.75 m, which was the shortest of all simulation conditions. As described in Section IV-A, the rotary LED transmitter rotates cylindrically to transmit information  $360^\circ$  in all directions. Due to the cylindrical rotation, LED lights overlap on both sides of the captured image. When we set  $\alpha$  to  $120^\circ$ , the number of overlapped LEDs was higher than in the other three conditions. It was difficult to recognize the blinking states of the overlapped LEDs, thus reducing the demodulation performance.

We now focus on the other BER curves of  $\alpha = 90^\circ$ ,  $60^\circ$ , and  $45^\circ$ . As indicated in Fig. 11, the error-free transmission distance of  $\alpha = 90^\circ$  was approximately 2.25 m while that of  $\alpha = 60^\circ$  and  $45^\circ$  was approximately 2.75 m for both. When we limited the data transmission angular range, the number of overlapping LEDs decreased, leading to a longer error-free transmission distance. However, we observed that setting the value of  $\alpha$  to  $45^\circ$  did not increase the error-free transmission distance compared with  $\alpha = 60^\circ$ . Therefore, we concluded that the error-free transmission distance was no longer related to  $\alpha$  when  $\alpha$  is less than  $60^\circ$ . To ensure the maximum error-free transmission distance while maximizing the data transmission rate, setting  $\alpha$  to  $60^\circ$  was the most suitable value in this study.

In addition, we observed that there were only slight differences in the BER of each curve when the communication distance was longer than 3.0 m. Therefore, we concluded that when the communication distance increases, the main factor affecting the demodulation performance is no longer  $\alpha$ . We believe that the demodulation performance at this point is mainly influenced by the parameter  $\Delta\theta$ . In this study, we set the value of  $\Delta\theta$  to  $1^\circ$  and evaluated the demodulation performance for our proposed transmitter.

## VI. EXPERIMENT

### A. Experimental Conditions

Table III presents the parameters of the experiment. This experiment was conducted indoors under a ceiling light during the daytime. On the transmitter side, based on the simulation results, we set the parameters  $\alpha$  and  $\Delta\theta$  to  $60^\circ$  and  $1^\circ$ , respectively. The rotation speed of the rotary LED transmitter



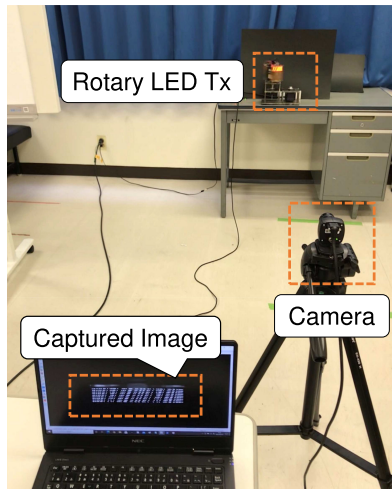


Fig. 12. Experimental setup. The experiment was conducted in an indoor environment. The rotary LED transmitter and receiver camera were arranged in a straight line. We set the communication distance from 0.5 to 4.0 m.

was set to 300 rotations per minute (rpm). In this experiment, we obtained the position of the transmitter and the coordinate of the afterimage of each LED light on the captured image in advance and applied these data as the known information. To highlight the transmitter, we also positioned a black board behind the transmitter. To measure the BER in the experiment, the M-sequence [31] was used for the random signal generator to generate the transmitting data. The LEDs blinked while moving across the front of the camera lens. The experimental setup is presented in Fig. 12.

On the receiver side, a complementary metal oxide semiconductor (CMOS) camera was used. We used a lens with a focal length of 35 mm and fixed the aperture of the lens at F8. The shooting speed of the camera was set to 5 fps. In addition, an ND8 filter was used to prevent the saturation of the LED light received by the camera. We set the communication distance from 0.5 to 4.0 m, transmitted 30780 bits of data every 0.5 m, and measured the BER at each distance. In this experiment, the camera recorded a video of the rotary LED transmitter that was rotating and blinking. Subsequently, we extracted images (i.e., frames) one by one from the recorded video and demodulated the data using these images.

### B. Experimental Result

Fig. 13 presents the BER plotted against the communication distance with constant  $\alpha (= 60^\circ)$  and constant  $\Delta\theta (= 1^\circ)$ . In this figure, the experimental result is compared with the simulation result. Fig. 13 indicates that the error-free transmission distance of the rotary LED transmitter in the experiment exceeded 2.5 m, which approximated the simulation result. When the communication distance was 3.0 m, the experimental BER was approximately  $1.0 \times 10^{-3}$ , which was more than one order of magnitude lower than the simulation result. We consider that the reason for this is the difference in the area of the LED light on the image due to the amount of light received. In the experiment, we prevented the saturation of the received LED light by adding an ND8 filter to the lens and setting the aperture

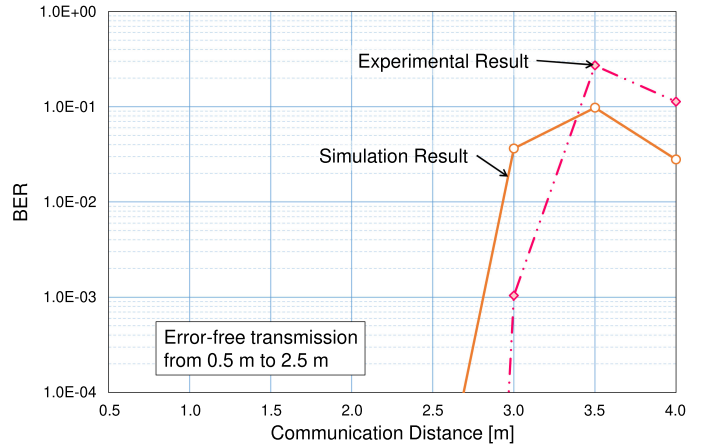


Fig. 13. BER versus communication distance ( $\alpha = 60^\circ$ ,  $\Delta\theta = 1^\circ$ ). The experimental and simulation results are compared.

to F8. In this case, the received LED light was focused on a few pixels on the image, and the receiver easily distinguished the afterimages of the LED lights at each angle despite the presence of the background light noise. Conversely, in the simulation, the received LED lights were degraded by blurring with a 2D Gaussian filter to simulate the optical spatial channel, but we did not assume the light aperture. In our opinion, this difference appeared in the simulation and experimental results. Consequently, the BER of 3.0 m in the experiment was lower than that in the simulation. When the communication distance exceeded 3.5 m, the experimental BER was over  $1.0 \times 10^{-1}$  while that in the simulation was less than  $1.0 \times 10^{-1}$ . This was because it became difficult to focus the lens with an increase in the communication distance. The unfocused lens caused the LED light source in the image to be blurred, thereby reducing the demodulation performance, especially at 4.0 m.

In addition, we observed that the BER at 4.0 m was lower than that at 3.5 m in both the simulation and experiment. We believe that this phenomenon was caused by cylindrical rotation motion. To provide an intuitive explanation of the reason, we assume that the LEDs alternate between ON and OFF every  $1^\circ$ . Fig. 14 presents ideal images generated at communication distances of 3.5 and 4.0 m. Here, the term *ideal image* is a pseudo-image generated based on the projection model described in Section IV-B and parameters in Table II. The horizontal interval of the LEDs was smaller than the vertical interval; therefore, we believe that the interference of LED light mainly originated from the horizontal direction (i.e., the rotation direction). In the cylindrical rotation motion, the width of the LED light in the image mainly depended on the rotation angle and was influenced by the physical size of the LEDs and pixels. For example, the width of  $1^\circ$  of LED light in the center of the afterimages of the LED lights was large whereas that at the edges of the image was small. With an increase in the communication distance, the width of the LED light decreased. When the size of the LED light in the image was so small that it was close to one pixel, the captured images resembled Fig. 14. As seen in Fig. 14, the LED lights at 3.5 m had the same width in the range of  $\pm 37^\circ$  from the center of the

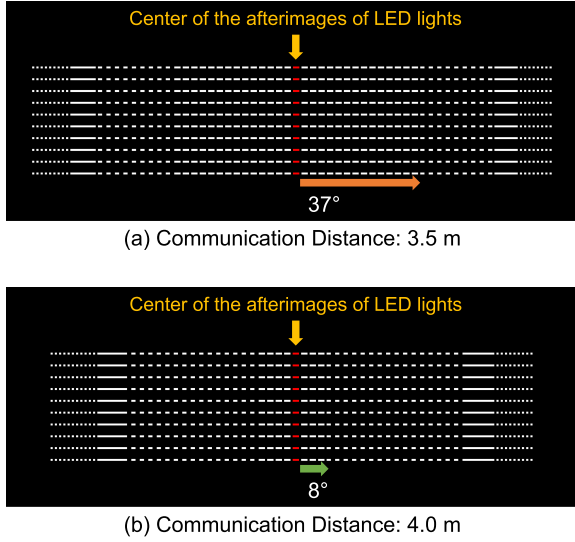


Fig. 14. Ideal images generated at a distance of 3.5 and 4.0 m. LEDs alternate between ON and OFF every  $1^\circ$  in ideal images.

afterimages. In contrast, at 4.0 m, the LED lights had the same width in the range of  $\pm 8^\circ$  from the center of the afterimages. The decreased width of the LED light indicates less light interference from adjacent rotating angles, thus allowing the blinking of LEDs to be distinguished easily. As illustrated in Fig. 14, the width of the LED light decreased starting at  $37^\circ$  and  $8^\circ$  when the distance was 3.5 and 4.0 m, respectively. When the data transmission angular range  $\alpha$  was set to  $60^\circ$ , the blinking of LEDs captured at 4.0 m was easier to distinguish than those captured at 3.5 m, thus leading to an increase in demodulation performance. Although there were several differences between the experimental and simulation results, the trends of the BER curves were almost the same. Therefore, we believe that both the simulations and experiments provided valid evaluations of the data demodulation capability of our proposed system.

Now, we focus on the data transmission rate of the rotary LED transmitter. Let  $S_r$  [rpm] denote the rotation speed of the transmitter. As mentioned in Section III-B, it takes the same time for the transmitter to perform one rotation as it does for the camera to capture an image. In this study, we define this time as the period of one signal transmission and denote it with  $\Delta t$ , which is calculated as follows:

$$\Delta t = \frac{60}{S_r}. \quad (8)$$

Let  $N_L$  denote the number of LEDs used in the transmitter. The data transmission rate of the rotary LED transmitter using OOK as the modulation method is denoted by  $R_{OOK}$ , which is calculated as follows:

$$R_{OOK} = \frac{N_L \cdot \alpha}{\Delta t \cdot \Delta \theta}. \quad (9)$$

With the parameters used in this experiment, the calculated  $R_{OOK}$  was 2.7 kbps ( $= 9 \text{ bits} \times 60^\circ / (0.2 \text{ s} \times 1^\circ)$ ). Note that in the conventional method, the positions of the LEDs are fixed. When nine LEDs were used to transmit data using OOK, the calculated data transmission rate of the conventional method was 45 bps ( $= 9 \text{ bits} / 0.2 \text{ s}$ ). Therefore, we can conclude

TABLE IV  
COMPARISON OF THE COMMUNICATION SPEED OF THE CONVENTIONAL AND PROPOSED METHODS

Number of LEDs ( $N_L$ )	9	9	18
Data angular range ( $\alpha$ )	$60^\circ$	$60^\circ$	$60^\circ$
Blinking angle ( $\Delta \theta$ )	$1^\circ$	$1^\circ$	$0.5^\circ$
Time of a rotation ( $\Delta t$ )	0.2 s	0.02 s	0.02 s
Conventional method	45 bps	450 bps	450 bps
Proposed method ( $R_{OOK}$ )	2.7 kbps	27 kbps	108 kbps
Increasing rate	60	60	240

that the proposed rotary LED transmitter has a higher data transmission rate than conventional methods when using the same number of LEDs.

In addition, the data transmission rate of the proposed transmitter depends on the rotation speed of the transmitter ( $S_r$ ), the number of LEDs ( $N_L$ ), the angular range of data transmission ( $\alpha$ ), and the LED blinking angle ( $\Delta \theta$ ). By increasing  $S_r$ ,  $N_L$ , and  $\alpha$  or decreasing  $\Delta \theta$ , the data transmission rate of the rotary LED transmitter can be further improved. For example, the data transmission rate was increased by setting  $N_L$  to 18,  $\Delta \theta$  to  $0.5^\circ$ , and  $\Delta t$  to 0.02 s. In this case, the predicted  $R_{OOK}$  of the proposed method is 108 kbps while that of the conventional method is 450 bps, as illustrated in Table IV. The predicted data transmission rate of the proposed method could be thus 240 times that of the conventional method. Therefore, the rotary LED transmitter has significant potential for data transmission rate improvement.

Herein, we compared the proposed method with the rolling shutter-type ISC scheme. As described in Section II-A, the rolling shutter-type ISC scheme uses the line-scan mechanism of the rolling shutter camera to improve the data rate. However, this scheme requires the light from the LED to be received over a large area of the sensor to achieve a high data transmission rate. This indicates that the data transmission rate depends on the area of the LED light that the LED receives on the camera. Measures such as shortening the communication distance between the LED transmitter and the receiver as much as possible are required to increase the LED light area.

By contrast, the proposed method increases the apparent number of LEDs captured per image by rotating a small number of LEDs to create an afterimage for increasing the transmission rate. The afterimages can be distinguished as long as there is at least one pixel in the image; hence, it does not depend on the LED area, unlike the rolling shutter-type ISC. Therefore, even if the communication distance between the transmitter and receiver is not much, the transmission speed can be sufficiently improved by using the rotary LED transmitter as long as each afterimage can be distinguished. At present, the communication rate in this experiment is lower than that of the rolling shutter-type ISC scheme shown in Section II-A. However, as shown in Table IV, we expect to achieve higher data transmission rate than the rolling shutter-type ISC scheme by changing the parameters  $N_L$ ,  $\alpha$ ,  $\Delta \theta$ , and  $\Delta t$ . Moreover,

the proposed method can improve the data transmission rate independent of the shutter type of the camera. In other words, the rotary LED transmitter has the advantage of improving the data transmission rate regardless of the shutter type of the camera.

## VII. CONCLUSION

In this paper, we focused on a transmitting device and developed a rotary LED transmitter for ISC. This transmitter rotates LEDs and simultaneously blinks them to transfer optical signals using the afterimages of LED lights. We convert the blinking of the LEDs from the time axis to the spatial axis of an image. Using the rotary LED transmitter, the shooting speed of the receiver camera does not have to match the blinking speed of the LED. Therefore, even with a commercial camera with a low shooting speed, the proposed method can increase the speed of ISC. As demonstrated by the simulation and experimental results, the ISC system using the rotary LED transmitter achieved 60 times faster data transmission than the conventional ISC system.

We believe that the rotary LED transmitter can be utilized in persistence of vision displays [32] and rotating lights such as the lamps attached to police cars. In addition, the proposed transmitter can be attached to devices with rotating mechanisms. Although our transmitter is currently in the prototype stage, it is a promising solution for various applications.

## ACKNOWLEDGMENT

The authors would like to thank Prof. Takaya Yamazato (Nagoya University), Prof. Toshiaki Fujii (Nagoya University), Prof. Hiraku Okada (Nagoya University), Prof. Koji Kamakura (Chiba Institute of Technology), and Dr. Masayuki Kinoshita (Chiba Institute of Technology) for useful discussions and suggestions.

## REFERENCES

- [1] Y. K. Cheng and K. W. E. Cheng, "General study for using LED to replace traditional lighting devices," in *Proc. ICPESEA*, pp. 173–177, 2006.
- [2] M. R. Krames *et al.*, "Status and future of high-power light-emitting diodes for solid-state lighting," *J. Disp. Technol.*, vol. 3, no. 2, pp. 160–175, Jun. 2007.
- [3] T. Komine and M. Nakagawa, "Fundamental analysis for visible-light communication system using LED lights," *IEEE Trans. Consum. Electron.*, vol. 50, no. 1, pp. 100–107, Feb. 2004.
- [4] H. Elgala, R. Mesleh, and H. Haas, "Indoor optical wireless communication: Potential and state-of-the-art," *IEEE Commun. Mag.*, vol. 49, no. 9, pp. 56–62, Sep. 2011.
- [5] P. H. Pathak, X. Feng, P. Hu, and P. Mohapatra, "Visible light communication, networking, and sensing: A survey, potential and challenges," *IEEE Commun. Surv. Tut.*, vol. 17, no. 4, pp. 2047–2077, Sep. 2015.
- [6] H. Haas, "LiFi is a paradigm-shifting 5G technology," *Rev. Phys.*, vol. 3, pp. 26–31, Nov. 2018.
- [7] J. Armstrong, Y. A. Sekercioglu, and A. Neild, "Visible light positioning: A roadmap for international standardization," *IEEE Commun. Mag.*, vol. 51, no. 12, pp. 68–73, Dec. 2013.
- [8] J. Fang *et al.*, "High-speed indoor navigation system based on visible light and mobile phone," *IEEE Photon. J.*, vol. 9, no. 2, Apr. 2017, Art. no. 8200711.
- [9] R. Zhang, W. Zhong, Q. Kemao, and S. Zhang, "A single LED positioning system based on circle projection," *IEEE Photon. J.*, vol. 9, no. 4, Aug. 2017, Art. no. 7905209.
- [10] S. M. Mana *et al.*, "LiFi experiments in a hospital," in *Proc. OFC*, pp. 1–3, 2020.
- [11] S. Arai, M. Kinoshita, and T. Yamazato, "Optical wireless communication: A candidate 6G technology?," *IEICE Trans. Fundamentals*, vol. E 104-A, no. 1, pp. 227–234, Jan. 2021.
- [12] H. Kaushal and G. Kaddoum, "Underwater optical wireless communication," *IEEE Access*, vol. 4, pp. 1518–1547, Apr. 2016.
- [13] X. Lin, "Adaptive control for LED-based underwater wireless communications using visible light," *IEICE Trans. Fundamentals*, vol. E100-A, no. 1, pp. 185–193, Jan. 2017.
- [14] T. Sawa, N. Nishimura, K. Tojo, and S. Ito, "Practical performance and prospect of underwater optical wireless communication -results of optical characteristic measurement at visible light band under water and communication tests with the prototype modem in the sea-," *IEICE Trans. Fundamentals*, vol. E102-A, no. 1, pp. 156–167, Jan. 2019.
- [15] H. B. C. Wook, S. Haruyama, and M. Nakagawa, "Visible light communication with LED traffic lights using 2-dimensional image sensor," *IEICE Trans. Fundamentals*, vol. E 89-A, no. 3, pp. 654–659, Mar. 2006.
- [16] T. Yamazato *et al.*, "Image-sensor-based visible light communication for automotive applications," *IEEE Commun. Mag.*, vol. 52, no. 7, pp. 88–97, Jul. 2014.
- [17] T. Yamazato *et al.*, "Vehicle motion and pixel illumination modeling for image sensor based visible light communication," *IEEE J. Sel. Areas Commun.*, vol. 33, no. 9, pp. 1793–1805, Sep. 2015.
- [18] K. Kamakura, "Image sensors meet LEDs," *IEICE Trans. Commun.*, vol. E100-B, no. 6, pp. 917–925, Jun. 2017.
- [19] H. Okada, S. Sato, T. Wada, K. Kobayashi, and M. Katayama, "Preventing degradation of the quality of visual information in digital signage and image-sensor-based visible light communication systems," *IEEE Photon. J.*, vol. 10, no. 3, Jun. 2018, Art. no. 7903509.
- [20] T. Nguyen, A. Islam, T. Yamazato, and Y. M. Jang, "Technical issues on IEEE 802.15.7 m image sensor communication standardization," *IEEE Commun. Mag.*, vol. 56, pp. 213–218, Feb. 2018.
- [21] Z. Liu, W. Guan, and S. Wen, "Improved target signal source tracking and extraction method based on outdoor visible light communication using an improved particle filter algorithm based on cam-shift algorithm," *IEEE Photon. J.*, vol. 11, no. 6, Dec. 2019, Art. no. 7907520.
- [22] S. Arai, H. Matsushita, Y. Ohira, T. Yendo, D. He, and T. Yamazato, "Maximum likelihood decoding based on pseudo-captured image templates for image sensor communication," *NOLTA, IEICE*, vol. 10, no. 2, pp. 173–189, Apr. 2019.
- [23] Y. Ohira, T. Yendo, S. Arai, and T. Yamazato, "High performance demodulation method with less complexity for image-sensor communication," *Opt. Exp.*, vol. 27, no. 15, pp. 21565–21578, Jul. 2019.
- [24] Z. Tang, S. Arai, T. Yendo, D. He, and T. Yamazato, "Sequential maximum likelihood decoding incorporating reliability determination for image sensor communication," *IEICE ComEX*, vol. 9, no. 8, pp. 365–370, Aug. 2020.
- [25] C. Danakis, M. Afgani, G. Povey, I. Underwood, and H. Haas, "Using a CMOS camera sensor for visible light communication," in *Proc. IEEE Globecom Workshops*, 2012, pp. 1244–1248.
- [26] Y. Imai, T. Ebihara, K. Mizutani, and N. Wakatsuki, "High-speed visible light communication using combination of low-speed image sensor and polygon mirror," *IEICE Trans. Fundamentals*, vol. E 99-A, no. 1, pp. 263–270, Jan. 2016.
- [27] S. Arai, Z. Tang, A. Nakayama, H. Takada, and T. Yendo, "Implementation experiment of a rotary LED transmitter for improving the transmission rate for image sensor communication," in *Proc. IEEE Globecom Workshops*, 2020, pp. 1–6.
- [28] "International electrotechnical commission IEC 62943:2017 visible light beacon system for multimedia application," Mar. 2017, <https://bit.ly/3fWdTKF>.
- [29] R. Raskar, A. Agrawal, and J. Tumblin, "Coded exposure photography: Motion deblurring using fluttered shutter," *ACM Trans. Graph.*, pp. 795–804, Jul. 2006.
- [30] J. Guertin, M. McGuire, and D. Nowrouzezahrai, "A fast and stable feature-aware motion blur filter," in *Proc. HPG*, pp. 51–60, 2014.
- [31] S. W. Golomb and G. Gong, *Signal Design for Good Correlation: For Wireless Communication, Cryptography, and Radar*. Cambridge, U.K.: Cambridge Univ. Press, 2005.
- [32] W. H. Al-Natsheh, B. K. Hammad, and M. A. Abu Zaid, "Design and implementation of a cylindrical persistence of vision display," in *Proc. ICEEE*, pp. 215–219, 2019.